

From mergers to collapse: scalarisation dynamics in neutron star binaries

Llibert Aresté Saló,^{1,2,*} Ricard Aguilera-Miret,^{3,4,†} Miguel Bezares,^{5,6,‡} and Thomas P. Sotiriou^{5,6,7,§}

¹*Instituut voor Theoretische Fysica, KU Leuven. Celestijnenlaan 200D, B-3001 Leuven, Belgium.*

²*Leuven Gravity Institute, KU Leuven. Celestijnenlaan 200D, B-3001 Leuven, Belgium.*

³*University of Hamburg, Hamburger Sternwarte, Gojenbergsweg 112, 21029, Hamburg, Germany*

⁴*Institute of Applied Computing & Community Code (IAC3),
Universitat de les Illes Balears, Palma, E-07122, Spain*

⁵*Nottingham Centre of Gravity, Nottingham NG7 2RD, United Kingdom*

⁶*School of Mathematical Sciences, University of Nottingham,
University Park, Nottingham NG7 2RD, United Kingdom*

⁷*School of Physics and Astronomy, University of Nottingham,
University Park, Nottingham NG7 2RD, United Kingdom*

We present the first fully non-linear evolutions of binary neutron star mergers in a moving-punctures approach in Einstein–scalar–Gauss–Bonnet gravity. We study both linear and quadratic-type couplings between the scalar and the Gauss-Bonnet invariant, and uncover new post-merger phenomena. These include an enhancement of the prompt collapse of a long-lived hyper-massive neutron star remnant and cases where the remnant develops a scalar configuration due to different scalarisation instabilities. This study initiates the exploration of beyond-General-Relativistic effects enhanced by the non-linear dynamics of the neutron star’s fluid.

Introduction.— The detection of Gravitational Waves (GWs) [1, 2] has opened a new observational window into the strong-field regime of gravity. The extreme gravitational potentials and spacetime curvatures during the coalescence of compact objects, which will be accessed with increasing precision by future detectors [3–7], offer us a promising prospect to test General Relativity (GR) and potentially observe new effects [8–11].

To fully exploit these detections, it is essential to obtain faithful theoretical predictions from well-motivated alternative theories of gravity. This motivates numerical simulations of compact object mergers in such scenarios. Attention has mostly focused on theories with an additional scalar field, as light scalars are ubiquitous in extensions of GR and the Standard Model. Several numerical studies of binary neutron star (BNS) mergers have been conducted in scalar-tensor theories of gravity within the class of theories developed by Damour and Esposito-Farèse [12–14] and in the presence of (kinetic) screening mechanisms [15–19].

Einstein–scalar–Gauss–Bonnet (EsGB) gravity, in which a scalar field couples to the Gauss-Bonnet curvature invariant, has also received a lot of attention recently, as this coupling is known to endow black holes (BHs) with scalar hair [20–24] and trigger highly non-linear strong gravity phenomena, such as scalarisation [25–29]. Taking into account no-hair theorems [24, 30–33], their known exceptions [20–23, 26, 27], and field redefinitions [34], the scalar-Gauss-Bonnet interaction can be seen as the most relevant term of an effective field theory (EFT) of gravity with an additional scalar in the strong field regime. Hence, EsGB gravity is among the few scenarios where strong-field deviations from GR could produce observable GW signatures that could be used to search for a new light field.

Couplings between a scalar and the Gauss-Bonnet invariant can change the character of the field equations as partial differential equations, as they modify their princi-

pal part (higher derivatives). This can render the initial value problem ill-posed in conventional formulations, in which case the theory would cease to be predictive. Early simulations circumvented this problem by working perturbatively in the coupling constant, e.g. [35–39]. Such simulations, however, suffer from secular growth of errors [37] and do not capture the full non-linear dynamics beyond GR.

It has been shown that introducing a modified harmonic gauge can lead to a well-posed formulation without the need for any perturbative treatment [40, 41]. The proof relies on the assumption that high-derivative contributions remain small compared to the GR terms, which is a well-motivated assumption from an EFT perspective. This framework has subsequently been adapted to singularity-avoiding, puncture-based gauge formulations through a modified conformal and covariant Z4 approach (mCCZ4) [42, 43]. These developments led to the first fully non-linear evolutions in such theories— in particular, in EsGB— for black hole spacetimes [44], followed later by others [42, 43, 45–54]. By contrast, the dynamics of neutron stars in EsGB remains still unexplored, with only two studies so far in the fully non-linear regime considering BNS [55] and BH-NS [56] systems.

In this paper, we present the first fully non-linear simulations of BNS mergers in EsGB gravity using a moving-puncture approach. We study the shift-symmetric sector of the theory, considering both BNS systems that form a long-lived hypermassive neutron star (HMNS) remnant and systems undergoing prompt collapse to a BH. We further identify configurations that form a long-lived HMNS in GR but collapse once the Gauss–Bonnet coupling exceeds a critical strength. Finally, we investigate a quadratic-type coupling and find spontaneous scalarisation triggered either by the mass of the HMNS remnant or by the spin of the newly formed BH.

We follow the conventions in [57]. Greek letters μ, ν, \dots denote spacetime indices. We set $G = c = 1$.

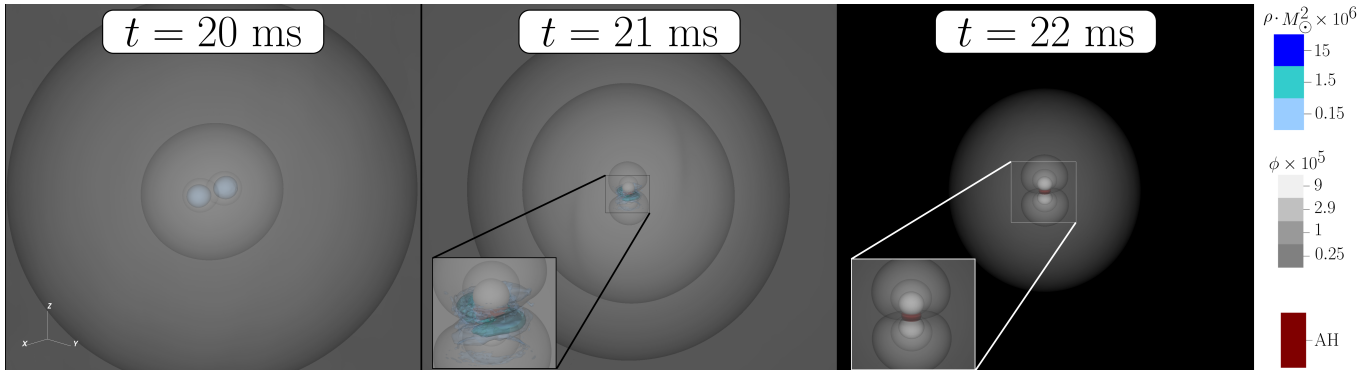


FIG. 1. *Spin-induced scalarisation of a BNS merger which promptly collapses to a BH.* Snapshots of the rest-mass fluid density (shades of blue) and scalar cloud (shades of grey) for a BNS merger in EsGB theory with a quadratic-type coupling of the form (2). The *left panel* shows the NSs during the late inspiral, which have a non-trivial scalar monopole. The *centre panel* displays the prompt collapse of the remnant to a BH, when some matter is engulfed by the BH, and this causes a reconfiguration of the scalar field. The *right panel* shows the final form of the remnant BH, with a scalar cloud that is stable due to the BH’s spin. The maroon contour indicates the location of the apparent horizon of the BH.

Theory.— The action of EsGB gravity reads

$$I = \int d^4x \sqrt{-g} \left[\frac{R}{16\pi} - \frac{1}{2} (\nabla\phi)^2 + \lambda f(\phi) \mathcal{L}_{\text{GB}} \right] + S_{\text{matter}}, \quad (1)$$

where λ is a coupling constant with dimensions of $[\text{length}]^2$, S_{matter} accounts for the neutron star’s fluid, $\mathcal{L}_{\text{GB}} = R^2 - 4R_{\mu\nu}R^{\mu\nu} + R_{\mu\nu\rho\sigma}R^{\mu\nu\rho\sigma}$ is the Gauss-Bonnet curvature, and $f(\phi)$ is an arbitrary function of the scalar field ϕ . We will take $f(\phi)$ to be either linear, i.e. $f(\phi) = \phi$, or quadratic-type, i.e. $f(\phi) = \phi^2/2 + \mathcal{O}(\phi^3)$.

A linear coupling corresponds to a shift-symmetric theory, in which constant shifts of the scalar field preserve the action [22, 23]. All compact objects in this theory are known to possess a non-trivial configuration of the scalar field, colloquially referred to as scalar hair. However, there is a notable difference between the scalar configuration of a BH and that of a NS. For BHs, the scalar exhibits the usual asymptotic fall-off, where ϕ_0 is the scalar field value at spatial infinity and Q_{SF} is the scalar monopole (or scalar charge).¹ For NSs $Q_{\text{SF}} = 0$, meaning that the fall-off of the scalar field is faster than $1/r$ [58]. This property of NSs in shift-symmetric EsGB gravity is essential for evading binary pulsar constraints.

A quadratic-type coupling function, namely $f(\phi) = \phi^2 + \mathcal{O}(\phi^3)$, leads to some drastic differences and a richer phenomenology. Firstly, there can be both $\phi = 0$ BHs and NSs stationary solutions that are identical to their GR counterparts, and scalarised solutions with $\phi \neq 0$, which deviate from GR [26–29, 59]. For the latter, both BHs and NSs have a non-zero scalar monopole (charge). For NSs, the Gauss-Bonnet invariant can take both positive and negative values within different regions of the NS, even for vanishing rotation. Therefore, scalarisation

can be triggered for both signs of the coupling constant [26]. Transitions between scalarised and unscalarised configurations can occur during the inspiral-merger-ringdown signal of binary compact objects [13, 43, 54, 60–62]. The specific form of the coupling function we will use here is

$$f(\phi) = \frac{1}{2\beta} (1 - e^{-\beta\phi^2}), \quad (2)$$

where β is a dimensionless parameter. This choice improves stability compared to the simpler $f(\phi) = \phi^2$ coupling [63–65].

Initial data and set-up.— All simulations are initialised from constraint-satisfying general-relativistic initial data for the metric and fluid variables, constructed using the LORENE [66] package. The scalar field is then consistently superposed on these data, and the full EsGB system is then evolved dynamically. For shift-symmetric EsGB gravity, we initialise the scalar field by setting $\phi = \partial_t\phi = 0$, which constitutes a valid solution of the shift-symmetric theory at the level of the initial data. During the subsequent evolution, the system experiences a short initial relaxation phase in which the neutron stars dynamically acquire a non-trivial configuration of the scalar field. This transient can slightly affect the orbital dynamics of the inspiral. Unless otherwise stated, this initial relaxation phase is not shown in the figures. For quadratic-type couplings, we instead initialise the scalar field with $\partial_t\phi = 0$ and a small Gaussian seed $\phi = A \exp[-(r - r_0)^2/(2\sigma^2)]$, with $\sigma = 1$, $A = 10^{-5}$, and $r_0 = 90 M_\odot$, in order to trigger the scalarisation instability. The resulting constraint violations are mild and efficiently damped during the initial transient by the CCZ4 formulation.

We consider both isolated NSs and BNS systems. Single NSs are placed at the centre of the numerical domain and evolved for several values of the mass and angular momentum. Binary systems are initialised at coordinate separations of either 45 or 50 km, depending on the total

¹ For clarity, we will use the term monopole, rather than charge, for the rest of the paper, to emphasise that higher multipoles are non-zero.

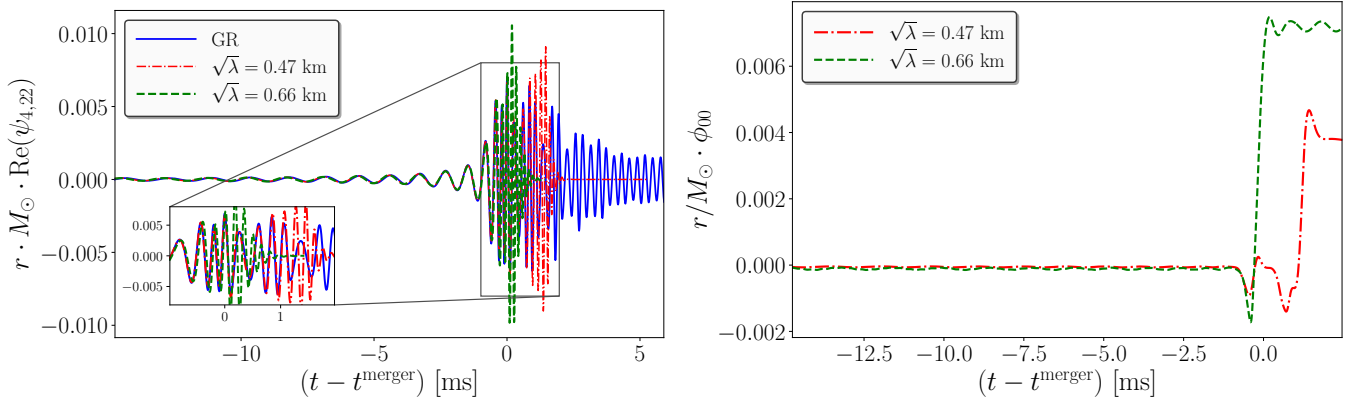


FIG. 2. *Prompt collapse of a BNS merger to a BH enhanced by shift-symmetric EsGB gravity.* The left panel shows the $(2, 2)$ mode of the Newman-Penrose Ψ_4 scalar of the GW, while the right panel displays the $(0, 0)$ mode of the scalar field, both extracted at $r = 100M_\odot$. We consider two values of the coupling constant: for the weaker one, the collapse occurs after the formation of the HMNS remnant, whereas for the stronger one, it occurs as soon as the merger occurs. The scalar monopole only becomes non-zero after the appearance of the BH.

mass, allowing for several orbits prior to merger. We focus on equal-mass BNS configurations with ADM masses $M_{\text{ADM}} = \{2.7, 2.6, 3.0\}M_\odot$, such that the first two cases do not undergo prompt collapse in GR, while the last case does. The corresponding initial orbital angular frequencies are $\Omega = \{1774.68, 1738.42, 1597.35\} \text{ rad s}^{-1}$, as summarised in Table I. In all simulations, the neutron stars are modelled using a tabulated piecewise-polytropic representation of the zero-temperature APR4 equation of state. Finally, constructing fully constraint-satisfying initial data for generic scalar-field configurations in EsGB gravity remains an open problem, although promising progress has recently been made [67, 68]. Further details on the formulation, numerical implementation, and code validation are provided in the Appendix.

TABLE I. *Parameters of the BNS simulations presented*

	(m_1, m_2) [M_\odot]	Initial separation [km]	Initial angular frequency [rad s $^{-1}$]
I	(1.35, 1.35)	45	1774.68
II	(1.3, 1.3)	45	1738.42
III	(1.5, 1.5)	50	1597.35

The coupling constant values used for shift-symmetric EsGB BNS systems are $\lambda = \{0.1, 0.2\}M_\odot^2$ corresponding to $\sqrt{\lambda} = \{0.47, 0.66\} \text{ km}$. These values are slightly larger than the current most stringent observational bounds on the theory, which come from comparing the black hole-neutron star GW signal GW230529 to Post-Newtonian (PN) results for EsGB, yielding a constraint of $\sqrt{\lambda} \lesssim 0.28 \text{ km}$ [69]. The fact that these bounds are based on the assumption that PN is valid up to merger, which was recently shown not to always be the case [52], justifies this choice. For quadratic-type couplings we instead use $\lambda = \{150, -90\}M_\odot^2$ corresponding to $\sqrt{|\lambda|} = \{18.05, 13.98\} \text{ km}$, which we can compare to the current observational limits for pulsars studied in [70]. For the positive value of the coupling, the bounds range from 11.43 to 26.05 km

depending on the EoS, although slightly higher values are also allowed, as pointed out in [71], where it was shown that strongly disfavoured values start at $\sqrt{\lambda} \gtrsim 41.27 \text{ km}$. Finally, for a negative coupling, the corresponding constraint for the APR4 EoS yields $\sqrt{|\lambda|} \lesssim 7.36 \text{ km}$, which is only slightly below the value considered.

Shift-symmetric EsGB binary neutron stars.—

We consider BNS mergers in shift-symmetric EsGB for the three types of initial data shown in Table I. In the left panel of Fig. 2, we show the GW signal of a BNS system that leads to a long-lived HMNS remnant in GR but collapses into a BH in EsGB once the coupling constant exceeds a critical value, corresponding to case I of Table I. This could be a smoking-gun signature of beyond GR physics. We note that this initial data is chosen to lie close to the prompt collapse threshold. As a result, the additional scalar radiation efficiently extracts angular momentum from the system, destabilising the HMNS remnant.

As we commented on earlier, NSs in shift-symmetric theory—in contrast to BHs—have no scalar monopole. Therefore, the dephasing of the gravitational wave with respect to GR is expected to be negligible. This is consistent with the left panel of Fig. 2, where waveforms have been aligned at the peak of the merger. However, longer waveforms with a more controlled eccentricity and higher resolution would be needed to perform a robust alignment and find out whether the effect recently found in [52] can also hold in BNS systems.

In the right panel of Fig. 2, we show the behaviour of the $(0, 0)$ mode of the scalar waves for the EsGB simulations corresponding to case I of Table I, which collapse into a BH. It clearly shows how the inspiral NSs have no scalar monopole, while this ramps up as soon as a BH is formed. We note that the small oscillations observed during the inspiral are very likely caused by the artificial initial transient going from zero to a non-zero scalar field. This induces oscillations in the fundamental fluid mode of

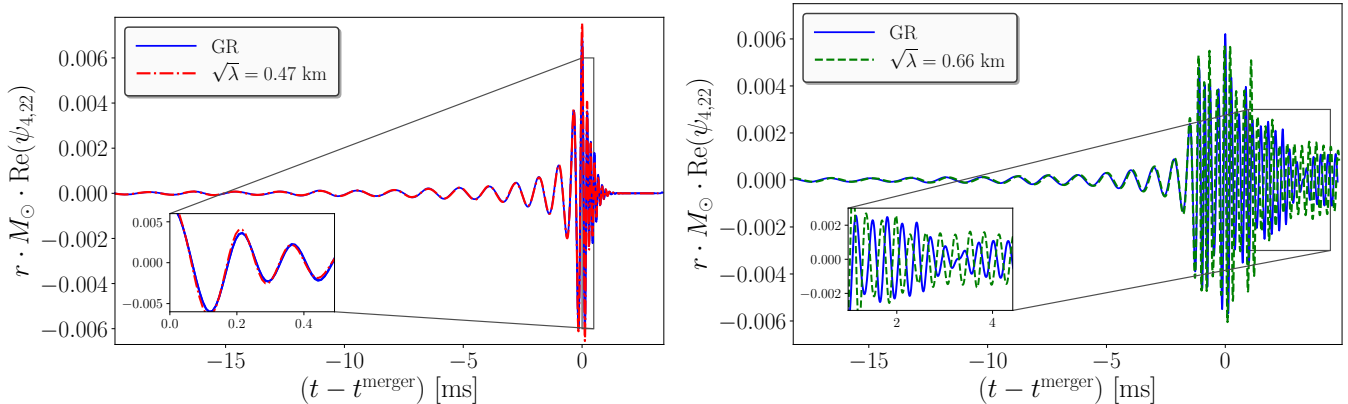


FIG. 3. Here we show the gravitational waveforms for BNS systems, both in GR and beyond, with higher (*left*) and lower (*right*) total mass with respect to the system in Fig. 2. Both GR and EsGB systems on the left promptly collapse into a BH with no visible dephasing, likely due to the lack of scalar monopole of the NSs. Both systems on the right lead to a long-lived HMNS remnant with some visible differences in the post-merger signal.

the star (f-mode) [55], which backreacts on the monopolar charge of the scalar field.

Fig. 3 displays cases for a lower and higher total mass, corresponding to cases II and III of Table I, respectively. The low-mass configuration forms a long-lived HMNS remnant in both GR and non-GR, whereas the high-mass undergoes prompt collapse for both cases. These results are perfectly consistent with the ones in [55]. We further note that similar differences in the post-merger signal to those shown in the right panel are also observed for different EoS (see, e.g., [72]), which we will study in more detail in future work.

Finally, we have explored the behaviour of the BNS systems for slightly higher coupling values. We have seen that for coupling constants $\sqrt{\lambda} = 0.95$ km and 1.34 km, we can evolve consistently throughout all of the inspiral, but we find a loss of hyperbolicity at the merger, both for systems collapsing to a BH and for those with a long-lived HMNS remnant NS. These values do coincide with the threshold of hyperbolicity observed for isolated black holes when normalised by the system’s total mass. However, since the hyperbolicity bounds for BBH are dominated by the smaller object, this means that the threshold for $\lambda/(m_1+m_2)^2$ in shift-symmetric EsGB BNS systems is $(1+q)^2$ times larger than in BBH systems, with $q = m_2/m_1 > 1$ being the unequal mass ratio.

Scalarisation.— We next consider quadratic-type couplings of the form of (2), which can lead to the phenomenon of “spontaneous scalarisation” [29]. As discussed above, NSs can undergo scalarisation for both signs of the coupling λ . Moreover, the scalarisation threshold depends on the spin as well. We start by investigating the scalarisation of isolated NSs for positive λ , as this will be useful for interpreting other results. The development of a scalar monopole over retarded time $u \equiv t - r_{\text{ex}} - 2M_{\odot} \log(r_{\text{ex}}/(2M_{\odot}) - 1)$ (with $r_{\text{ex}} = 100M_{\odot}$ the extraction radius) is shown in Fig. 4. For non-spinning NSs configurations, it develops faster and reaches higher

values for more massive NSs, in agreement with [73]. For the value of the coupling considered here, the theoretical threshold mass is $M = 1.57M_{\odot}$,² and this is consistent with Fig. 4, where an NS of mass $M = 1.59M_{\odot}$ experiences scalarisation, while one of $M = 1.52M_{\odot}$ does not. We next consider spinning NSs with a fixed dimensionless spin, $J/M^2 \approx 0.45$, and examine several mass values. We find that the threshold mass for scalarisation is higher for spinning NSs, lying between $1.63M_{\odot}$ and $1.73M_{\odot}$. This behaviour is expected for $\lambda > 0$, as rotation reduces the central fluid energy density, thereby weakening the scalarisation instability.

We now turn our attention to BNS mergers. In the left panel of Fig. 5, we show the evolution of the scalar monopole for a BNS system whose merger leads to a long-lived HMNS remnant, with $\lambda > 0$. While the scalar monopole remains zero during the inspiral, scalarisation takes place post-merger. The HMNS formed by the merger is more massive than the inspiral NSs, so its fluid energy density is large enough to trigger the instability responsible for scalarisation. Hence, we attribute the scalarisation of the increase in mass of the NSs remnant, rather than to the spin-induced scalarisation found for BBH systems [28, 43, 59, 74]. Our simulations verify predictions obtained using perturbation theory and stationary solutions of NSs in EsGB gravity with quadratic-type couplings [73].

Finally, we consider the opposite sign of the coupling constant λ and evolve a BNS that promptly collapses into a BH. We choose such values for λ and for the NS masses so that the BH remnant would have scalar hair due to spin-induced scalarisation. Indeed, our simulations capture this phenomenon for the first time. The scalar monopole is shown in the right panel of Fig. 5. For the NS masses and value of λ we have chosen, the inspiral

² We thank Nicola Franchini for having computed this value with his static spherically symmetric code.

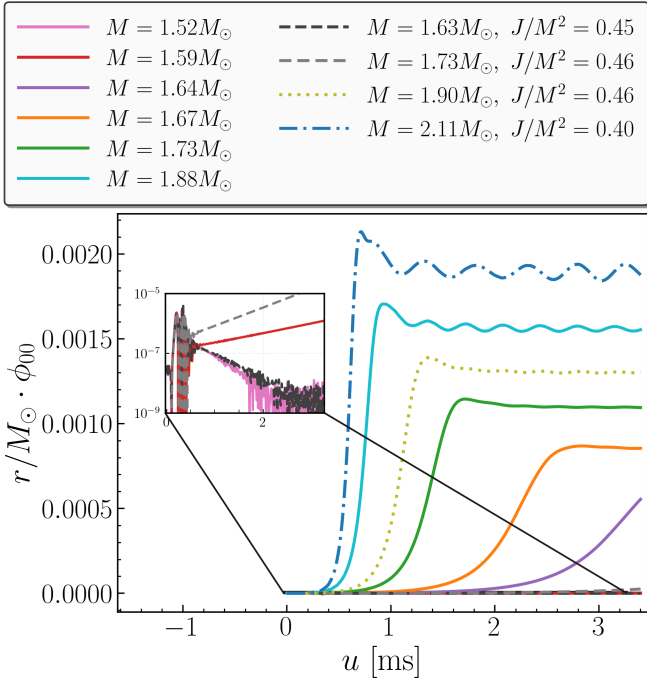


FIG. 4. *Spontaneous scalarisation of single NSs in EsGB with a quadratic-type coupling.* We have considered several values of neutron star’s masses and spins with the coupling constants of $\lambda = 150M_{\odot}^2$ and $\beta = 400 \cdot 16\pi$. This plot shows that the threshold mass of scalarisation increases significantly for a large spin. See the Appendix for convergence of the spinning NS with higher mass.

NSs are scalarised. The scalar monopole exhibits oscillations during the inspiral due to the initial transient and drops sharply at prompt collapse as the fluid energy density, which supports the NSs scalar configuration, is lost. Then, the scalar monopole grows again as a result of a spin-induced scalarisation of the BH. Several time snapshots of the three-dimensional configuration of the scalar cloud around this system are shown in Fig. 1. Near the remnant BH, the scalar takes larger values around the poles of the apparent horizon, as these are regions where the Gauss-Bonnet invariant is negative and the scalarisation instability is hence stronger. This is consistent with the results of [43].

Conclusions.— We present the first fully non-linear binary neutron star merger evolutions using a moving-punctures approach in Einstein–scalar–Gauss–Bonnet gravity. For this purpose, we have implemented the modified CCZ4 formulation [42] in the MHDuet code [75], demonstrating that such systems can be evolved robustly in the fully non-linear regime. These simulations include additional physical scenarios with respect to earlier studies [55] and reveal several new signatures of beyond GR physics in the GW signals of BNS mergers.

We have studied both systems that lead to a long-lived HMNS remnant and to a prompt collapse of the remnant to a BH, for both linear and quadratic-type couplings. For linear couplings, NSs do not have a scalar monopole, leav-

ing the inspiral phase effectively indistinguishable from GR even for significantly large values of the coupling constant. Nevertheless, our simulations show that smoking-gun signatures can arise during the merger phase, such as the prompt collapse to a BH for systems that would otherwise form a long-lived HMNS in GR. A systematic exploration of the dependence of the post-merger signal on the NS equation of state is left for future work.

Quadratic-type couplings instead give rise to a much richer phenomenology, including nonlinear phenomena associated with scalarisation [29]. Our simulations captured for the first time two such phenomena. The first one is the scalarisation of the long-lived HMNS remnant after the merger of two unscalarised NSs. The second is the prompt descalarisation after the merger of scalarised NSs, followed by a spin-induced scalarisation of a remnant BH.

This study provides a basis for studying further interesting signatures of beyond GR effects enhanced by the dynamics of the neutron star’s fluid, which can only be captured in the fully non-linear regime and complements the effects recently seen in [50, 52] in vacuum spacetimes. Further work is required to improve the initial data and eliminate the transient effect in the fluid’s f-mode, which is especially important in cases where the NSs have scalar monopole. In future work, we plan to complete the picture by studying BH-NS systems and incorporating the effect of magnetic fields.

Acknowledgments.— We thank Katy Clough, Nicola Franchini, Ludovico Machet, Borja Miñano and Carlos Palenzuela for useful discussions. In the early stages of this work LAS was supported by a London Mathematical Society (LMS) Early Career Fellowship. RAM is funded by the Deutsche Forschungsgemeinschaft (DFG, German Research Foundation) under the Germany Excellence Strategy - EXC 2121 ‘Quantum Universe’ - 390833306 and by the European Research Council (ERC) Advanced Grant INSPIRATION under the European Union’s Horizon 2020 research and innovation program (grant agreement no. 101053985). MB acknowledges partial support from the STFC Consolidated Grant nos. ST/Z000424/1 and UKRI2492. TPS acknowledges partial support from the STFC Consolidated Grant nos. ST/V005596/1, ST/X000672/1, and UKRI2492. This work used the DiRAC Memory Intensive service Cosma8 at Durham University, managed by the Institute for Computational Cosmology on behalf of the STFC DiRAC HPC Facility (www.dirac.ac.uk). The DiRAC service at Durham was funded by BEIS, UKRI and STFC capital funding, Durham University and STFC operations grants. DiRAC is part of the UKRI Digital Research Infrastructure. We used the resources provided by the VSC (Flemish Supercomputer Center), funded by the Research Foundation - Flanders (FWO) and the Flemish Government. We acknowledge the computing time made available to us on the high-performance computer ‘Lise’ at the NHR Centre NHR@ZIB. This center is jointly supported by the Federal Ministry of Education and Research and the state governments participating in the NHR.

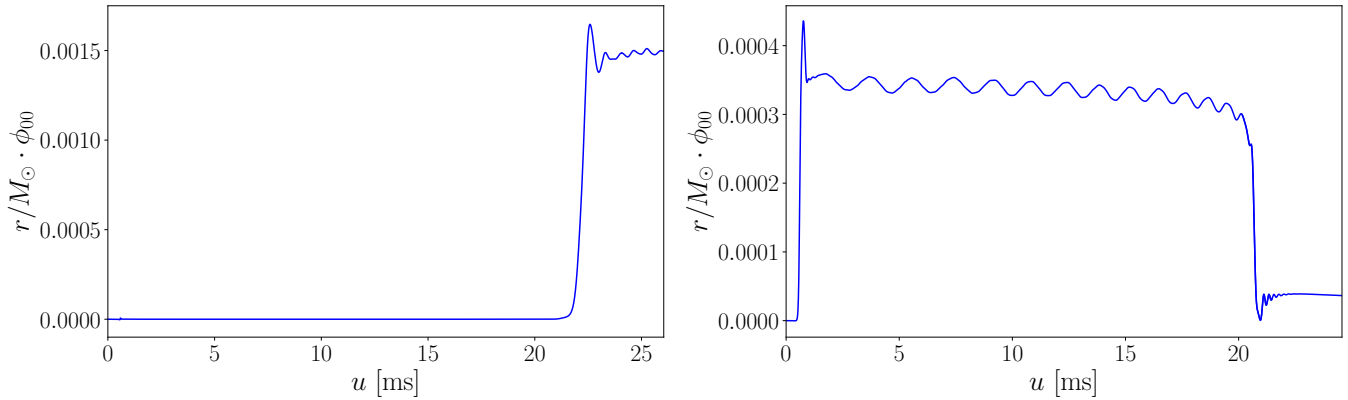


FIG. 5. *BNS merger in EsGB gravity with quadratic-type coupling.* The left panel shows the evolution of the scalar monopole for a BNS merger leading to a long-lived HMNS remnant in which the scalar field only develops after merger because of the larger mass of the remnant for the coupling values of $\lambda = 150M_{\odot}^2$ and $\beta = 400 \cdot 16\pi$. The right panel considers instead the case of a BNS merger promptly collapsing to a BH shown in Fig. 1, for the coupling values of $\lambda = -90M_{\odot}^2$ and $\beta = 2000 \cdot 16\pi$.

* llibert.arestesalo@kuleuven.be

† ricard.aguilera.miret@uni-hamburg.de

‡ miguel.bezaresfigueroa@nottingham.ac.uk

§ thomas.sotiriou@nottingham.ac.uk

- [1] B. P. Abbott *et al.* (LIGO Scientific, Virgo), Observation of Gravitational Waves from a Binary Black Hole Merger, *Phys. Rev. Lett.* **116**, 061102 (2016), [arXiv:1602.03837 \[gr-qc\]](https://arxiv.org/abs/1602.03837).
- [2] B. P. Abbott *et al.* (LIGO Scientific, Virgo), GW170817: Observation of Gravitational Waves from a Binary Neutron Star Inspiral, *Phys. Rev. Lett.* **119**, 161101 (2017), [arXiv:1710.05832 \[gr-qc\]](https://arxiv.org/abs/1710.05832).
- [3] M. Colpi *et al.* (LISA), LISA Definition Study Report, (2024), [arXiv:2402.07571 \[astro-ph.CO\]](https://arxiv.org/abs/2402.07571).
- [4] M. Punturo *et al.*, The Einstein Telescope: A third-generation gravitational wave observatory, *Class. Quant. Grav.* **27**, 194002 (2010).
- [5] M. Maggiore *et al.* (ET), Science Case for the Einstein Telescope, *JCAP* **03**, 050, [arXiv:1912.02622 \[astro-ph.CO\]](https://arxiv.org/abs/1912.02622).
- [6] A. Abac *et al.* (ET), The Science of the Einstein Telescope, (2025), [arXiv:2503.12263 \[gr-qc\]](https://arxiv.org/abs/2503.12263).
- [7] D. Reitze *et al.*, Cosmic Explorer: The U.S. Contribution to Gravitational-Wave Astronomy beyond LIGO, *Bull. Am. Astron. Soc.* **51**, 035 (2019), [arXiv:1907.04833 \[astro-ph.IM\]](https://arxiv.org/abs/1907.04833).
- [8] L. Barack *et al.*, Black holes, gravitational waves and fundamental physics: a roadmap, *Class. Quant. Grav.* **36**, 143001 (2019), [arXiv:1806.05195 \[gr-qc\]](https://arxiv.org/abs/1806.05195).
- [9] E. Barausse *et al.*, Prospects for Fundamental Physics with LISA, *Gen. Rel. Grav.* **52**, 81 (2020), [arXiv:2001.09793 \[gr-qc\]](https://arxiv.org/abs/2001.09793).
- [10] K. G. Arun *et al.* (LISA), New horizons for fundamental physics with LISA, *Living Rev. Rel.* **25**, 4 (2022), [arXiv:2205.01597 \[gr-qc\]](https://arxiv.org/abs/2205.01597).
- [11] V. Kalogera *et al.*, The Next Generation Global Gravitational Wave Observatory: The Science Book, (2021), [arXiv:2111.06990 \[gr-qc\]](https://arxiv.org/abs/2111.06990).
- [12] E. Barausse, C. Palenzuela, M. Ponce, and L. Lehner, Neutron-star mergers in scalar-tensor theories of gravity, *Phys. Rev. D* **87**, 081506 (2013), [arXiv:1212.5053 \[gr-qc\]](https://arxiv.org/abs/1212.5053).
- [13] C. Palenzuela, E. Barausse, M. Ponce, and L. Lehner, Dynamical scalarization of neutron stars in scalar-tensor gravity theories, *Phys. Rev. D* **89**, 044024 (2014), [arXiv:1310.4481 \[gr-qc\]](https://arxiv.org/abs/1310.4481).
- [14] M. Shibata, K. Taniguchi, H. Okawa, and A. Buonanno, Coalescence of binary neutron stars in a scalar-tensor theory of gravity, *Phys. Rev. D* **89**, 084005 (2014), [arXiv:1310.0627 \[gr-qc\]](https://arxiv.org/abs/1310.0627).
- [15] L. ter Haar, M. Bezares, M. Crisostomi, E. Barausse, and C. Palenzuela, Dynamics of Screening in Modified Gravity, *Phys. Rev. Lett.* **126**, 091102 (2021), [arXiv:2009.03354 \[gr-qc\]](https://arxiv.org/abs/2009.03354).
- [16] M. Bezares, L. ter Haar, M. Crisostomi, E. Barausse, and C. Palenzuela, Kinetic screening in nonlinear stellar oscillations and gravitational collapse, *Phys. Rev. D* **104**, 044022 (2021), [arXiv:2105.13992 \[gr-qc\]](https://arxiv.org/abs/2105.13992).
- [17] M. Bezares, R. Aguilera-Miret, L. ter Haar, M. Crisostomi, C. Palenzuela, and E. Barausse, No Evidence of Kinetic Screening in Simulations of Merging Binary Neutron Stars beyond General Relativity, *Phys. Rev. Lett.* **128**, 091103 (2022), [arXiv:2107.05648 \[gr-qc\]](https://arxiv.org/abs/2107.05648).
- [18] M. Shibata and D. Traykova, Properties of scalar wave emission in a scalar-tensor theory with kinetic screening, *Phys. Rev. D* **107**, 044068 (2023), [arXiv:2210.12139 \[gr-qc\]](https://arxiv.org/abs/2210.12139).
- [19] R. Cayuso, A. Kuntz, M. Bezares, and E. Barausse, Scalar emission from neutron star-black hole binaries in scalar-tensor theories with kinetic screening, *Phys. Rev. D* **110**, 104071 (2024), [arXiv:2410.16367 \[gr-qc\]](https://arxiv.org/abs/2410.16367).
- [20] P. Kanti, N. E. Mavromatos, J. Rizos, K. Tamvakis, and E. Winstanley, Dilatonic black holes in higher curvature string gravity, *Phys. Rev. D* **54**, 5049 (1996), [arXiv:hep-th/9511071](https://arxiv.org/abs/hep-th/9511071).
- [21] N. Yunes and L. C. Stein, Non-Spinning Black Holes in Alternative Theories of Gravity, *Phys. Rev. D* **83**, 104002 (2011), [arXiv:1101.2921 \[gr-qc\]](https://arxiv.org/abs/1101.2921).
- [22] T. P. Sotiriou and S.-Y. Zhou, Black hole hair in generalized scalar-tensor gravity, *Phys. Rev. Lett.* **112**, 251102 (2014), [arXiv:1312.3622 \[gr-qc\]](https://arxiv.org/abs/1312.3622).
- [23] T. P. Sotiriou and S.-Y. Zhou, Black hole hair in generalized scalar-tensor gravity: An explicit example, *Phys. Rev. D* **90**, 124063 (2014), [arXiv:1408.1698 \[gr-qc\]](https://arxiv.org/abs/1408.1698).
- [24] T. P. Sotiriou, Black Holes and Scalar Fields, *Class. Quant. Grav.* **32**, 214002 (2015), [arXiv:1505.00248 \[gr-qc\]](https://arxiv.org/abs/1505.00248).
- [25] T. Damour and G. Esposito-Farese, Nonperturbative

- strong field effects in tensor - scalar theories of gravitation, *Phys. Rev. Lett.* **70**, 2220 (1993).
- [26] H. O. Silva, J. Sakstein, L. Gualtieri, T. P. Sotiriou, and E. Berti, Spontaneous scalarization of black holes and compact stars from a Gauss-Bonnet coupling, *Phys. Rev. Lett.* **120**, 131104 (2018), [arXiv:1711.02080 \[gr-qc\]](#).
- [27] D. D. Doneva and S. S. Yazadjiev, New Gauss-Bonnet Black Holes with Curvature-Induced Scalarization in Extended Scalar-Tensor Theories, *Phys. Rev. Lett.* **120**, 131103 (2018), [arXiv:1711.01187 \[gr-qc\]](#).
- [28] A. Dima, E. Barausse, N. Franchini, and T. P. Sotiriou, Spin-induced black hole spontaneous scalarization, *Phys. Rev. Lett.* **125**, 231101 (2020), [arXiv:2006.03095 \[gr-qc\]](#).
- [29] D. D. Doneva, F. M. Ramazanoğlu, H. O. Silva, T. P. Sotiriou, and S. S. Yazadjiev, Spontaneous scalarization, *Rev. Mod. Phys.* **96**, 015004 (2024), [arXiv:2211.01766 \[gr-qc\]](#).
- [30] S. W. Hawking, Black holes in the Brans-Dicke theory of gravitation, *Commun. Math. Phys.* **25**, 167 (1972).
- [31] J. D. Bekenstein, Novel “no-scalar-hair” theorem for black holes, *Phys. Rev. D* **51**, R6608 (1995).
- [32] T. P. Sotiriou and V. Faraoni, Black holes in scalar-tensor gravity, *Phys. Rev. Lett.* **108**, 081103 (2012), [arXiv:1109.6324 \[gr-qc\]](#).
- [33] L. Hui and A. Nicolis, No-Hair Theorem for the Galileon, *Phys. Rev. Lett.* **110**, 241104 (2013), [arXiv:1202.1296 \[hep-th\]](#).
- [34] S. Weinberg, Effective Field Theory for Inflation, *Phys. Rev. D* **77**, 123541 (2008), [arXiv:0804.4291 \[hep-th\]](#).
- [35] R. Benkel, T. P. Sotiriou, and H. Witek, Black hole hair formation in shift-symmetric generalised scalar-tensor gravity, *Class. Quant. Grav.* **34**, 064001 (2017), [arXiv:1610.09168 \[gr-qc\]](#).
- [36] R. Benkel, T. P. Sotiriou, and H. Witek, Dynamical scalar hair formation around a Schwarzschild black hole, *Phys. Rev. D* **94**, 121503 (2016), [arXiv:1612.08184 \[gr-qc\]](#).
- [37] M. Okounkova, L. C. Stein, M. A. Scheel, and D. A. Hemberger, Numerical binary black hole mergers in dynamical Chern-Simons gravity: Scalar field, *Phys. Rev. D* **96**, 044020 (2017), [arXiv:1705.07924 \[gr-qc\]](#).
- [38] H. Witek, L. Gualtieri, P. Pani, and T. P. Sotiriou, Black holes and binary mergers in scalar Gauss-Bonnet gravity: scalar field dynamics, *Phys. Rev. D* **99**, 064035 (2019), [arXiv:1810.05177 \[gr-qc\]](#).
- [39] M. Okounkova, L. C. Stein, M. A. Scheel, and S. A. Teukolsky, Numerical binary black hole collisions in dynamical Chern-Simons gravity, *Phys. Rev. D* **100**, 104026 (2019), [arXiv:1906.08789 \[gr-qc\]](#).
- [40] Á. D. Kovács and H. S. Reall, Well-Posed Formulation of Scalar-Tensor Effective Field Theory, *Phys. Rev. Lett.* **124**, 221101 (2020), [arXiv:2003.04327 \[gr-qc\]](#).
- [41] Á. D. Kovács and H. S. Reall, Well-posed formulation of Lovelock and Horndeski theories, *Phys. Rev. D* **101**, 124003 (2020), [arXiv:2003.08398 \[gr-qc\]](#).
- [42] L. Aresté Saló, K. Clough, and P. Figueras, Well-Posedness of the Four-Derivative Scalar-Tensor Theory of Gravity in Singularity Avoiding Coordinates, *Phys. Rev. Lett.* **129**, 261104 (2022), [arXiv:2208.14470 \[gr-qc\]](#).
- [43] L. Aresté Saló, K. Clough, and P. Figueras, Puncture gauge formulation for Einstein-Gauss-Bonnet gravity and four-derivative scalar-tensor theories in d+1 space-time dimensions, *Phys. Rev. D* **108**, 084018 (2023), [arXiv:2306.14966 \[gr-qc\]](#).
- [44] W. E. East and J. L. Ripley, Evolution of Einstein-scalar-Gauss-Bonnet gravity using a modified harmonic formulation, *Phys. Rev. D* **103**, 044040 (2021), [arXiv:2011.03547 \[gr-qc\]](#).
- [45] W. E. East and J. L. Ripley, Dynamics of Spontaneous Black Hole Scalarization and Mergers in Einstein-Scalar-Gauss-Bonnet Gravity, *Phys. Rev. Lett.* **127**, 101102 (2021), [arXiv:2105.08571 \[gr-qc\]](#).
- [46] M. Corman, J. L. Ripley, and W. E. East, Nonlinear studies of binary black hole mergers in Einstein-scalar-Gauss-Bonnet gravity, *Phys. Rev. D* **107**, 024014 (2023), [arXiv:2210.09235 \[gr-qc\]](#).
- [47] D. D. Doneva, L. Aresté Saló, K. Clough, P. Figueras, and S. S. Yazadjiev, Testing the limits of scalar-Gauss-Bonnet gravity through nonlinear evolutions of spin-induced scalarization, *Phys. Rev. D* **108**, 084017 (2023), [arXiv:2307.06474 \[gr-qc\]](#).
- [48] D. D. Doneva, L. Aresté Saló, and S. S. Yazadjiev, 3+1 nonlinear evolution of Ricci-coupled scalar-Gauss-Bonnet gravity, *Phys. Rev. D* **110**, 024040 (2024), [arXiv:2404.15526 \[gr-qc\]](#).
- [49] M. Corman, L. Lehner, W. E. East, and G. Dideron, Nonlinear studies of modifications to general relativity: Comparing different approaches, *Phys. Rev. D* **110**, 084048 (2024), [arXiv:2405.15581 \[gr-qc\]](#).
- [50] G. Lara *et al.*, Signatures from metastable oppositely-charged black hole binaries in scalar Gauss-Bonnet gravity, (2025), [arXiv:2505.14785 \[gr-qc\]](#).
- [51] L. Aresté Saló, D. D. Doneva, K. Clough, P. Figueras, and S. S. Yazadjiev, Challenges in the nonlinear evolution of unequal mass binaries in scalar-Gauss-Bonnet gravity, *Phys. Rev. D* **112**, 084022 (2025), [arXiv:2507.13046 \[gr-qc\]](#).
- [52] M. Corman, L. Aresté Saló, and K. Clough, Black hole binaries in shift-symmetric Einstein-scalar-Gauss-Bonnet gravity experience a slower merger phase, (2025), [arXiv:2511.19073 \[gr-qc\]](#).
- [53] H. L. H. Shum, L. Aresté Saló, F. Thaalba, M. Bezares, and T. P. Sotiriou, A well-posed BSSN-type formulation for scalar-tensor theories of gravity with second-order field equations, (2025), [arXiv:2512.11034 \[gr-qc\]](#).
- [54] L. Capuano, L. Aresté Saló, D. D. Doneva, S. S. Yazadjiev, and E. Barausse, Dynamical hair growth in black hole binaries in Einstein-scalar-Gauss-Bonnet gravity, (2026), [arXiv:2602.02650 \[gr-qc\]](#).
- [55] W. E. East and F. Pretorius, Binary neutron star mergers in Einstein-scalar-Gauss-Bonnet gravity, *Phys. Rev. D* **106**, 104055 (2022), [arXiv:2208.09488 \[gr-qc\]](#).
- [56] M. Corman and W. E. East, Black hole-neutron star mergers in Einstein-scalar-Gauss-Bonnet gravity, *Phys. Rev. D* **110**, 084065 (2024), [arXiv:2405.18496 \[gr-qc\]](#).
- [57] R. M. Wald, *General Relativity* (Chicago Univ. Pr., Chicago, USA, 1984).
- [58] K. Yagi, L. C. Stein, and N. Yunes, Challenging the Presence of Scalar Charge and Dipolar Radiation in Binary Pulsars, *Phys. Rev. D* **93**, 024010 (2016), [arXiv:1510.02152 \[gr-qc\]](#).
- [59] C. A. R. Herdeiro, E. Radu, H. O. Silva, T. P. Sotiriou, and N. Yunes, Spin-induced scalarized black holes, *Phys. Rev. Lett.* **126**, 011103 (2021), [arXiv:2009.03904 \[gr-qc\]](#).
- [60] H. O. Silva, H. Witek, M. Elley, and N. Yunes, Dynamical Descalarization in Binary Black Hole Mergers, *Phys. Rev. Lett.* **127**, 031101 (2021), [arXiv:2012.10436 \[gr-qc\]](#).
- [61] M. Elley, H. O. Silva, H. Witek, and N. Yunes, Spin-induced dynamical scalarization, descalarization, and stealthness in scalar-Gauss-Bonnet gravity during a black hole coalescence, *Phys. Rev. D* **106**, 044018 (2022), [arXiv:2205.06240 \[gr-qc\]](#).
- [62] H.-J. Kuan, A. T.-L. Lam, D. D. Doneva, S. S. Yazadjiev, M. Shibata, and K. Kiuchi, Dynamical scalarization during neutron star mergers in scalar-Gauss-Bonnet the-

- ory, *Phys. Rev. D* **108**, 063033 (2023), arXiv:2302.11596 [gr-qc].
- [63] J. L. Blázquez-Salcedo, D. D. Doneva, J. Kunz, and S. S. Yazadjiev, Radial perturbations of the scalarized Einstein-Gauss-Bonnet black holes, *Phys. Rev. D* **98**, 084011 (2018), arXiv:1805.05755 [gr-qc].
- [64] H. O. Silva, C. F. B. Macedo, T. P. Sotiriou, L. Gualtieri, J. Sakstein, and E. Berti, Stability of scalarized black hole solutions in scalar-Gauss-Bonnet gravity, *Phys. Rev. D* **99**, 064011 (2019), arXiv:1812.05590 [gr-qc].
- [65] C. F. B. Macedo, J. Sakstein, E. Berti, L. Gualtieri, H. O. Silva, and T. P. Sotiriou, Self-interactions and Spontaneous Black Hole Scalarization, *Phys. Rev. D* **99**, 104041 (2019), arXiv:1903.06784 [gr-qc].
- [66] LORENE, LORENE home page (2010), <http://www.lorene.obspm.fr/>.
- [67] S. E. Brady, L. Aresté Saló, K. Clough, P. Figueras, and A. P. S., Solving the initial conditions problem for modified gravity theories, *Phys. Rev. D* **108**, 104022 (2023), arXiv:2308.16791 [gr-qc].
- [68] P. J. Nee, G. Lara, H. P. Pfeiffer, and N. L. Vu, Quasistationary hair for binary black hole initial data in scalar Gauss-Bonnet gravity, *Phys. Rev. D* **111**, 024061 (2025), arXiv:2406.08410 [gr-qc].
- [69] E. M. Säger *et al.*, Tests of General Relativity with GW230529: a neutron star merging with a lower mass-gap compact object, (2024), arXiv:2406.03568 [gr-qc].
- [70] V. I. Danchev, D. D. Doneva, and S. S. Yazadjiev, Constraining scalarization in scalar-Gauss-Bonnet gravity through binary pulsars, *Phys. Rev. D* **106**, 124001 (2022), arXiv:2112.03869 [gr-qc].
- [71] L. K. Wong, C. A. R. Herdeiro, and E. Radu, Constraining spontaneous black hole scalarization in scalar-tensor-Gauss-Bonnet theories with current gravitational-wave data, *Phys. Rev. D* **106**, 024008 (2022), arXiv:2204.09038 [gr-qc].
- [72] M. Llorens-Monteagudo, A. Torres-Forné, and J. A. Font, Classification of the equation of state of neutron stars via sparse dictionary learning, (2025), arXiv:2512.16441 [astro-ph.HE].
- [73] D. D. Doneva, C. J. Krüger, K. V. Staykov, and P. Y. Yordanov, Neutron stars in Gauss-Bonnet gravity: Non-linear scalarization and gravitational phase transitions, *Phys. Rev. D* **108**, 044054 (2023), arXiv:2306.16988 [gr-qc].
- [74] E. Berti, L. G. Collodel, B. Kleihaus, and J. Kunz, Spin-induced black-hole scalarization in Einstein-scalar-Gauss-Bonnet theory, *Phys. Rev. Lett.* **126**, 011104 (2021), arXiv:2009.03905 [gr-qc].
- [75] C. Palenzuela *et al.*, MHDuet: a high-order general relativistic radiation MHD code for CPU and GPU architectures, *Class. Quant. Grav.* **42**, 245005 (2025), arXiv:2510.13965 [gr-qc].
- [76] L. Aresté Saló, S. E. Brady, K. Clough, D. Doneva, T. Evstafyeva, P. Figueras, T. França, L. Rossi, and S. Yao, GRFolres: A code for modified gravity simulations in strong gravity, *J. Open Source Softw.* **9**, 6369 (2024), arXiv:2309.06225 [gr-qc].
- [77] T. Andrade *et al.*, GRChombo: An adaptable numerical relativity code for fundamental physics, *J. Open Source Softw.* **6**, 3703 (2021), arXiv:2201.03458 [gr-qc].
- [78] C. Palenzuela, B. Miñano, D. Viganò, A. Arbona, C. Bona-Casas, A. Rigo, M. Bezares, C. Bona, and J. Massó, A Simflowny-based finite-difference code for high-performance computing in numerical relativity, *Classical and Quantum Gravity* **35**, 185007 (2018), arXiv:1806.04182 [physics.comp-ph].
- [79] MHDuet code website, <http://mhduet.liu.edu/> (2026).
- [80] A. Arbona, A. Artigues, C. Bona-Casas, J. Massó, B. Miñano, A. Rigo, M. Trias, and C. Bona, Simflowny: A general-purpose platform for the management of physical models and simulation problems, *Computer Physics Communications* **184**, 2321 (2013).
- [81] A. Arbona, B. Miñano, A. Rigo, C. Bona, C. Palenzuela, A. Artigues, C. Bona-Casas, and J. Massó, Simflowny 2: An upgraded platform for scientific modelling and simulation, *Computer Physics Communications* **229**, 170 (2018), arXiv:1702.04715 [cs.MS].
- [82] R. D. Hornung and S. R. Kohn, Managing application complexity in the samrai object-oriented framework, *Concurrency and Computation: Practice and Experience* **14**, 347 (2002).
- [83] B. T. Gunney and R. W. Anderson, Advances in patch-based adaptive mesh refinement scalability, *Journal of Parallel and Distributed Computing* **89**, 65 (2016).
- [84] W. Zhang, A. Almgren, V. Beckner, J. Bell, J. Blaschke, C. Chan, M. Day, B. Friesen, K. Gott, D. Graves, M. Katz, A. Myers, T. Nguyen, A. Nonaka, M. Rosso, S. Williams, and M. Zingale, AMReX: a framework for block-structured adaptive mesh refinement, *Journal of Open Source Software* **4**, 1370 (2019).
- [85] Overview of amrex gpu strategy (2025).
- [86] W. Zhang, A. Myers, K. Gott, A. Almgren, and J. Bell, Amrex: Block-structured adaptive mesh refinement for multiphysics applications, *The International Journal of High Performance Computing Applications* **35**, 508–526 (2021).
- [87] C.-W. Shu, Essentially non-oscillatory and weighted essentially non-oscillatory schemes for hyperbolic conservation laws (Springer Berlin Heidelberg, 1998) pp. 325–432, DOI:10.1007/BFb0096355.
- [88] A. Suresh and H. Huynh, Accurate monotonicity-preserving schemes with runge–kutta time stepping, *Journal of Computational Physics* **136**, 83 (1997).
- [89] P. McCorquodale and P. Colella, A high-order finite-volume method for conservation laws on locally refined grids, *Commun. Appl. Math. Comput. Sci.* **6**, 1 (2011).
- [90] B. Mongwane, Toward a consistent framework for high order mesh refinement schemes in numerical relativity, *General Relativity and Gravitation* **47**, 60 (2015), arXiv:1504.07609 [gr-qc].

Formulation and implementation

To evolve the fully non-linear EsGB equations of motion, we employ the modified conformal and covariant Z4 (mCCZ4) formalism [42], first implemented in GRFolres [76] (an extension of the GRChombo [77] numerical relativity code), which was shown to be well-posed in EsGB in the weakly coupling regime. In the same spirit as the modified harmonic gauge [40, 41], this formalism introduces two auxiliary metrics to ensure that gauge modes propagate with speeds distinct from the physical ones, defined as

$$\tilde{g}^{\mu\nu} = g^{\mu\nu} - a(x)n^\mu n^\nu, \quad \hat{g}^{\mu\nu} = g^{\mu\nu} - b(x)n^\mu n^\nu, \quad (3)$$

where $a(x)$ and $b(x)$ are arbitrary functions such that $0 < a(x) < b(x)$, and n^μ is the unit timelike vector normal to $t = \text{const}$. These choices modify the equations of motion both for the metric and gauge variables (see [42, 43] for further details); throughout this work we fix $a(x) = 0.2$ and $b(x) = 0.4$, following previous studies.

The EsGB equations in the mCCZ4 formulation are coupled to the general relativistic magnetohydrodynamic equations and evolved using the open-source code MHDuet [75, 78, 79], an evolution code for general relativistic magnetohydrodynamics with neutrino transport. The code is generated by the SIMFLOWNY platform [80, 81] from a high-level specification of the computational system, and can target either the SAMRAI infrastructure [82, 83] or, in newer versions, the AMREX framework [84–86] providing parallelisation and adaptive mesh refinement (AMR). The code employs a fourth-order-accurate finite-difference operator for the spatial derivatives in the metric and scalar field sectors (supplemented with sixth-order Kreiss–Oliger dissipation), a high-resolution shock-capturing (HRSC) scheme for the fluid based on Lax–Friedrichs flux splitting [87] and fifth-order MP5 reconstruction [88], and a fourth-order Runge–Kutta time integrator with time step $\Delta t \leq 0.4 \Delta x$. Refinement boundaries are treated efficiently and accurately when sub-cycling in time [89, 90]. A new version of MHDuet including the EsGB model, based on the AMREX infrastructure and supporting GPU acceleration, will be made open source and released in the near future in [79].

The binary is evolved in a cubic domain of size $[-1228, 1228]$ km in each direction. The inspiral is fully covered by six Fixed Mesh Refinement (FMR) levels. Each consists of a cube with twice the resolution of the next larger one. In addition, we use a single AMR level, covering regions where the density exceeds $5 \times 10^{12} \text{ g cm}^{-3}$ and providing a uniform resolution throughout the shear layer. When the HMNS remnant collapses into a BH, we instead cover the regions where the lapse is below 0.65. With this grid structure, we

achieve a maximum resolution of $\Delta x_{\min} = 120 \text{ m}$ covering at least the most dense region of the remnant.

Convergence test

In this section, we present the convergence test for the $(0,0)$ mode of the scalar field within the spontaneous scalarisation of a single NS shown in Fig. 4. In particular, we study the case with $M = 2.11M_\odot$ and $J/M^2 = 0.40$, which is close to the values attained by the HMNS remnant in a BNS merger system.

We consider three different resolutions, namely low (LR), medium (MR) and high (HR), corresponding to maximum resolutions of $\Delta x_{\min} = 240, 120$ and 60 m , respectively. The MR run uses the same set-up explained in the previous section, whereas one FMR level was added (subtracted) for the HR (LR) case.

Fig. 6 displays the difference across resolutions of the $(0,0)$ mode of the scalar field aligned at the time when the first peak occurs (corresponding to the maximum) and normalised with its value in the peak. It shows that the convergence order is approximately between 3rd and 4th order, with some mild over-convergence very likely due to the oscillatory nature of the observable we have considered. This is perfectly consistent with the order of the numerical schemes used. We have also verified that both the peak amplitude and the time required to reach it exhibit an order of convergence between 2.5 and 3, as expected due to the non-linearities arising during scalarisation.

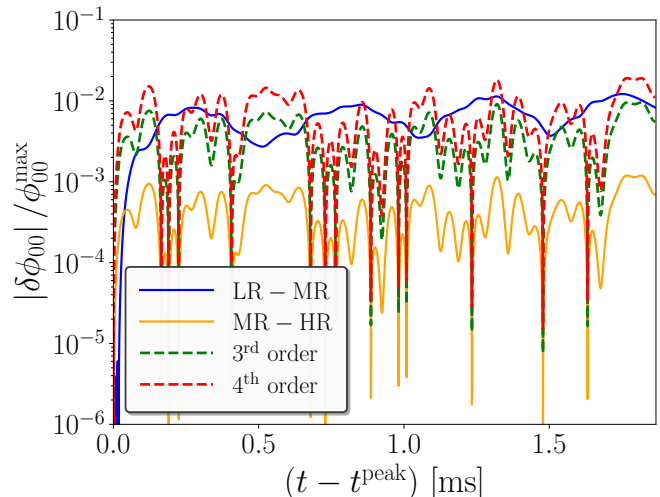


FIG. 6. *Convergence test.* We show the difference across resolutions of the $(0,0)$ mode of the scalar field for the spontaneous scalarisation of a spinning NS. The difference between the high and medium resolution runs has been rescaled by the convergence factor $Q_n = \frac{h_{LR}^n - h_{MR}^n}{h_{MR}^n - h_{HR}^n}$, assuming third and fourth order convergence.